ChemCatChem

Research Article
doi.org/10.1002/cctc.202301242

Chemistry Europe
European Chemical Societies Publishing

www.chemcatchem.org

The Influence of Melting on Catalysis in Propane Oxidation

Ezgi Erdem,[a, b] Andrey V. Tarasov,[a] Pierre Kube,[a] Gregor Koch,[a] Milivoj Plodinec,[a] Thomas Lunkenbein,[a] Spencer Carey,[a] Yuanqing Wang,[a] Michael Hävecker,[a, c] Frank Rosowski,[b, d] Robert Schlögl,[a] and Annette Trunschke*[a]

A model catalyst composed of crystalline potassium pentavanadate ($K_3V_5O_{14}$) supported on silica was studied to elucidate the effect of phase transitions on the performance of potassium-promoted vanadia catalysts in propane oxidation. Operando calorimetry shows a clear correlation between a drop in activity and an increase in selectivity to propylene upon melting of the crystalline $K_3V_5O_{14}$ phase under reaction conditions. The pentavanadate phase itself is not active in propane oxidation, neither in the solid nor in the molten state. The activity of the catalyst mainly originates from highly-active, i.e., unselective V_xO_y surface species anchored to silica and formed during synthesis in addition to the supported pentavanadate phase. Melting of $K_3V_5O_{14}$ leads to the coverage of these V_xO_y species preventing the overoxidation of propylene and leading to an increase in propylene selectivity. The change in catalyst properties is therefore due to a physical effect and not to a change in the chemical properties of the predominant crystalline phase.

Introduction

Since there are no binding counter atoms, the surface termination of solids usually deviates from the structure of the bulk. These distortions at the interface, in turn, lead to changes in the electronic properties of solids due to the formation of frustrated surface sites. If the solid is a heterogeneous catalyst, this can affect the catalytic activity, and superimpose trends and scaling relations expected based on the periodicity of bulk chemical features.[1–2]

In both oxidative dehydrogenation of propane and non-oxidative metathesis of propane over SiO_2-supported MoO_x catalysts carried out in a wide temperature range from 50 °C to 550 °C, an increase in reactivity was attributed to the appearance of strain in active silica-supported $(Si\text{-}O)_2Mo{=}O_2$ species.[3] However, due to their striving for an optimization of the bond strengths, surface atoms with directional bonds seek new equilibrium positions, leading to restructurings across different orders of length and time scales, which can result in the loss of strain and thus deactivation of the catalyst.[4] High temperature facilitates these processes, which can lead to phase transitions and melting of phases. In turn, liquefaction of a surface compound can result in the generation of the active phase in thermal catalysis, making the low-temperature state of a catalyst significantly different from the state after activation.[5] or under reaction conditions.[6–7] Restructuring can also be associated with non-linear dynamic phenomena.[8] Therefore, it is challenging to correlate catalyst dynamics experimentally with catalytic activity, particularly at high temperatures, as it requires examination of the catalyst under often very harsh working conditions.

Alkali metal oxides serve as promoters for a wide variety of catalysts. The bulk properties of the promoted catalysts may significantly differ from the unpromoted ones. For example, with vanadium oxide, an active phase in oxidation reactions, alkali vanadate phases can be formed, which can undergo phase transitions at elevated temperatures. Alkali oxides are also frequently used to promote supported vanadium oxide catalysts for propane oxidation (Figure 1). Here we investigate the influence of melting on the reactivity of alkali-promoted vanadium oxide catalysts in the oxidation of propane using operando flow calorimetry.

Vanadium oxide-based materials are among the most widely studied catalysts in the oxidative dehydrogenation of light alkanes such as propane.[14–19] Usually, due to secondary reactions of the olefin to undesired carbon oxides, the selectivity to propylene decreases sharply with increasing conversion and often reaches values below 50% at propane conversions above 10% (Figure 1).[14] Despite intensive studies over the past three decades, no significant improvement in propylene selectivity has been achieved, in particular because there is still no clear picture of relationships between surface

[a] E. Erdem, A. V. Tarasov, P. Kube, G. Koch, M. Plodinec, T. Lunkenbein, S. Carey, Y. Wang, M. Hävecker, R. Schlögl, A. Trunschke
Department of Inorganic Chemistry, Fritz-Haber-Institute der Max-Planck-Gesellschaft, Faradayweg 4–6 14195 Berlin, Germany
E-mail: trunschke@fhi-berlin.mpg.de

[b] E. Erdem, F. Rosowski
BasCat-UniCat BASF JointLab, Technical University Berlin, Sekr. EW K 01, Hardenbergstrasse 36, 10623 Berlin, Germany

[c] M. Hävecker
Max Planck Institute for Chemical Energy Conversion, postCode/>45470 Mülheim, Germany

[d] F. Rosowski
BASF SE, Catalysis Research, Carl-Bosch-Strasse 38, 67056 Ludwigshafen, Germany

Supporting information for this article is available on the WWW under https://doi.org/10.1002/cctc.202301242

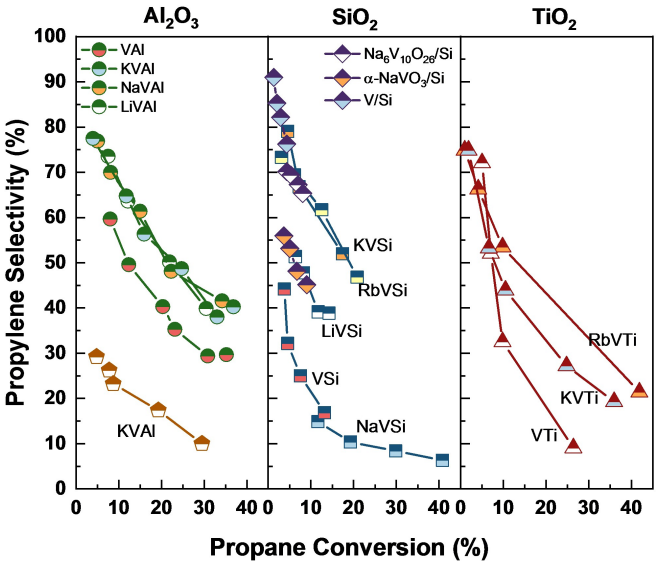

Figure 1. Typical reactivity profiles of alkali-containing supported vanadium oxide catalysts in propane oxidation ("○" adopted from, [9] "□"adopted from,[10] "△"adopted from [11] "◇"adopted from,[12] and "⌂" adopted from).[13]

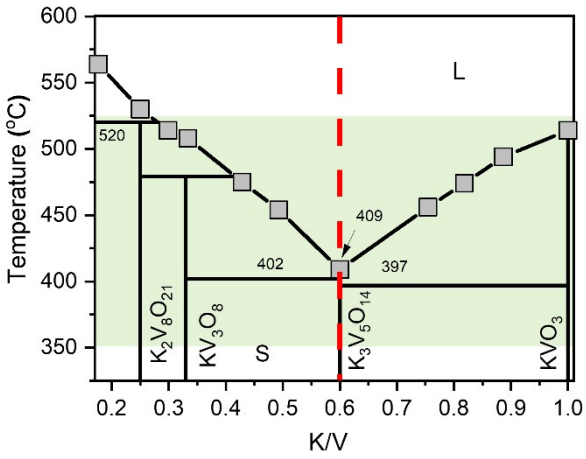

Figure 2. Phase diagram of K_2CO_3 and V_2O_5; The area marked in green indicates the applied reaction temperature range in the oxidative dehydrogenation of propane while the red dashed line indicates the studied K/V ratio (K/V = 0.6); Constructed with the combined data from literature.[41–42]

composition and structure of the catalysts and their reactivity.[19–21]

Most frequently, but not necessarily, the addition of alkali ions such as Li, Na, K, and Rb to supported vanadium oxide catalysts decreases the activity in propane oxidation while improves the selectivity to propylene (Figure 1).[9–11,22–32] The phenomena observed in catalysis were largely associated with changes in the molecular surface structures, *i.e.*, the relative abundance of monomeric and polymeric V_xO_y species,[9,31–33] and their dispersion.[9,31,34] Performance changes were also attributed to a change in acid-base properties. A decrease in acidity and an increase in basicity facilitate the desorption of propylene from the surface, so it has been suggested that the addition of alkali inhibits secondary reactions of propylene and thus total combustion.[9–10,22,27,30,35–37] Furthermore, a change in the redox properties upon alkali addition, *i.e.*, a decrease in reducibility was also observed.[9,11,22,28,38] All these various surface and volume properties are unfortunately interrelated, and there may be other factors that are important that have not been considered so far. For instance, the presence of alkali elements may cause the formation of alkali-vanadates (*e.g.*, KVO_3)[27] on the surface (Figure 2). However, in none of the previous studies was the activity of the alkali vanadate phases themselves tested for propane oxidation. The possible contribution of potentially formed alkali vanadate phases to catalysis are therefore unknown. In addition, alkali vanadates have low melting points (Figure 2), ranging from 400 °C to 550 °C, which is the typical temperature range for propane oxidation. None of the previous studies performed specific experiments based on which phase transitions such as melting were discussed as a factor that could affect the catalytic properties. This also applies to investigations in which at least local melting could have been possible due to the alkali content.[11,27,39–40]

In the present work, we have prepared a model catalyst to specifically study the effect of melting of an alkali vanadate phase on propane oxidation. We have found a direct correlation between melting and the change in catalytic properties. The findings shed new light on interpreting promoter effects in oxidation catalysis and the impact of catalyst dynamics on performance in general. In the following, it will be shown that the change in activity is not due to the crystalline phase, but to modifications of highly-active minority species, which can also be detected, for example, in silica-supported polyoxometalates.[43] It is therefore crucial to distinguish experimentally between observations attributed to the crystalline phase and the complexity of the real situation.

Results and Discussion

Synthesis and Characterization of the Model Catalyst

A potassium-containing silica-supported vanadium oxide catalyst was synthesized by considering the phase diagram of K_2CO_3 and V_2O_5 (Figure 2). The atomic ratio between K and V was chosen to be 0.6 to obtain a phase-pure $K_3V_5O_{14}$ surface phase (red dotted line in Figure 2). The catalyst will be denoted as K/V = 0.6 in the following. This means that if this catalyst was applied at typical reaction temperatures for propane oxidation between 400 and 500 °C, a phase transition from solid to liquid would occur if the supported phase behaved analogously to pure V_2O_5-K_2O mixtures.[41] To verify this, we first compared the phase transformation of the pure phase with that of its physical mixture with the support SiO_2 and the supported phase in an oxygen / argon gas mixture (Figure 3).

The catalyst (internal catalyst ID S28654) was prepared via spray-drying of an aqueous V_2O_5-K_2CO_3-SiO_2 suspension followed by calcination in air at 620 °C for 16 hours. Fumed silica (Aerosil 300, ID 28958) was used as support. The details of catalyst synthesis are explained in the experimental section.

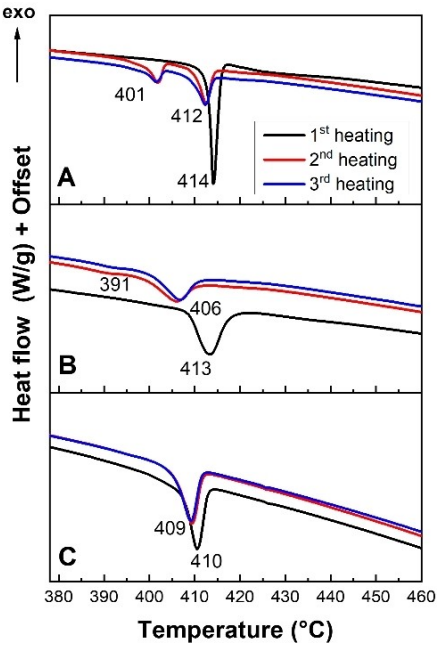

Figure 3. DSC profiles of the support-free $K_3V_5O_{14}$ (ID 31564) **(A)**, a physical mixture of $K_3V_5O_{14}$ and SiO_2 **(B)**, and the catalyst with K/V = 0.6 **(C)** measured under 21% O_2 / 79% Ar with a flow of 50 ml·min^{-1}, a heating rate of 10 °C·min^{-1}, and a cooling rate of 5 °C·min^{-1} in an alumina crucible with lid in the temperature range between 30 °C and 550 °C (data shown up to 460 °C).

Structural and chemical properties are summarized in Table S1 in the Supporting Information. A total metal oxide loading of 8.4 wt% was achieved, of which 6.4 wt% was accounted for V_2O_5. $K_3V_5O_{14}$ was the only crystalline phase that could be detected in the catalyst by powder X-ray diffraction (Figure S1 in the Supporting Information), which is in accordance with the phase diagram (Figure 2).[41]

Differential Scanning Calorimetry (DSC) indicates melting of the support-free $K_3V_5O_{14}$ phase at 414 °C (Figure 3A, black line). When the solidified melt was reheated in a second and third heating cycle after heating to 550 °C and cooling to room temperature it was found that the formation of an additional phase occurs. This is reflected in two endothermic signals at 401 °C and 412 °C in the second and third cycle (Figure 3A, red and blue lines). These peaks can be associated with the formation of potassium trivanadate KV_3O_8[42] during active cooling (5 °C·min^{-1}) owing to a narrow homogeneity range. Uniform solidification of $K_3V_5O_{14}$ follows slow kinetics and thus requires slower cooling rates than the applied one. The peak at 401 °C is close to the eutectic point for the mixture of $K_3V_5O_{14}$ and KV_3O_8 (Figure 2). The diffraction pattern measured at 50 °C before and after each heating cycle, however, showed $K_3V_5O_{14}$ as the only crystalline phase (Figure S2). Recrystallisation causes formation of differently oriented crystallites, which is reflected in changing signal intensities, but the $K_3V_5O_{14}$ phase is retained. Small diffraction peaks, which appear at about 31° 2θ in a high-temperature XRD experiment between 415–500 °C, indicate the presence of small amounts of KVO_3 (Figure S3).

In the physical mixture (Figure 3B) and in the catalyst (Figure 3C), the melting peak broadened, and the maximum observed in the first cycle (black curves) slightly shifted to lower temperatures possibly due to an impact of the particle size distribution of the supported phase and/or the interaction with the support. In the second and third melting cycles (red and blue curves), the endothermic signal for the newly formed phase in the physical mixture (Figure 3B) is much less pronounced than for the pure phase (Figure 3A) and not visible in the catalyst (Figure 3C). Hence, the supported phase demonstrates better thermal stability because there is no severe phase separation after recrystallization.

The difference between the bulk and the supported mixture suggests interaction at the interface between the potassium vanadate phase(s) and the silica support. Indeed, K $2p_{3/2}$ and $2p_{1/2}$ peaks at 293.7 and 296.4 eV, respectively, measured for K/V = 0.6 by XPS, indicate on the formation of potassium silicate,[44–45] implying that part of the potassium has dissolved in the support (Figure S4A and D in the Supporting Information). The second, more intense contribution in the K 2p spectra at lower binding energies (292 and 295 eV) is attributed to K in potassium vanadate (Figure S4B, C, E in the Supporting Information). The binding energies of V $2p_{3/2}$ core levels at 517.5 and 516.5 (±0.25) eV are characteristic of a mixture of V^{4+} and V^{5+} components (Figure S5 in the Supporting Information). The vanadium oxidation state of 4+ is not consistent with the potassium pentavanadate phase $K_3V_5O_{14}$ and suggests the presence of additional vanadium oxide species, although beam damage or partial loss of oxygen cannot be excluded as reason for the appearance of V^{4+} at the high measurement temperatures (520 °C) applied to reduce charging despite the presence of oxygen in the gas phase (Figure S5).

The reaction of silica with potassium and the blockage of pores by the potassium vanadate layer are responsible for a significant reduction of the specific surface area of the catalyst to 24 $m^2 \cdot g^{-1}$ compared to the pure silica support (Aerosil 300, 285 $m^2 \cdot g^{-1}$) (Table S1 in Supporting Information). The coverage of the surface of the spheric silica particles with a solidified melt is also clearly visible in the scanning electron micrographs (Figures 4 A and B). In the solid state, this phase does not entirely cover the silica surface. According to STEM-EDX (Figures 4 C–4 H), potassium and vanadium appear mainly together in the different regions of the catalyst surface, confirming the formation of the potassium vanadate phase (Figures 4 E and 4 F).

The ex-situ Raman spectrum of the catalyst recorded with an excitation wavelength of 532 nm (Figure S6 in the Supporting Information) is dominated by bands due to the $K_3V_5O_{14}$ phase, which agrees with XRD. When using an UV laser (266 nm), the spectrum differs and shows bands at wavenumbers > 1000 cm^{-1} (1024 and 1058 cm^{-1}) (Figure S7 in the Supporting Information) for both hydrated (fresh) and dehydrated (activated) states of the catalyst. These bands, and, in addition, the band at 838 cm^{-1} appearing at the dehydrated state could indicate the presence of dispersed vanadium oxide species V_xO_y with different degrees of oligomerization anchored directly to the silica support in addition to the $K_3V_5O_{14}$ phase.[46]

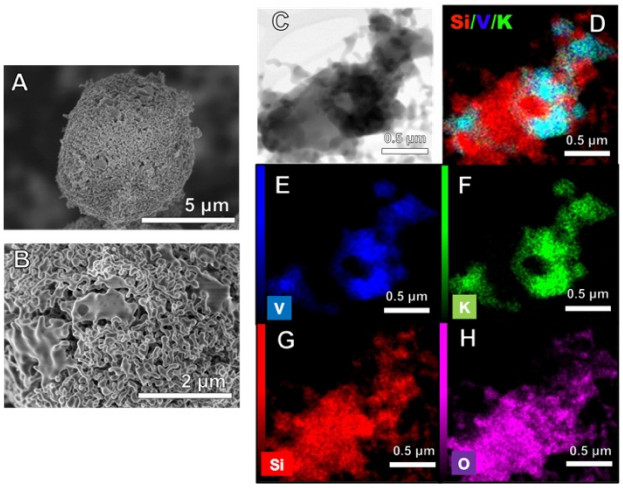

Figure 4. Representative SEM image of one spherical SiO_2 particle covered by K–V oxide **(A)**, and a magnified region of the solidified melt of the K/V = 0.6 catalyst **(B)**. TEM image of the solidified K-V oxide melt on SiO_2 **(C)**, and elemental mapping with STEM-EDS **(D–H)**.

Operando Differential Scanning Calorimetry

Melting was not only found in synthetic air (Figure 3), but could directly be detected under the reaction conditions of propane oxidation using operando DSC (Figures 5 A–C). Given the exothermicity of propane oxidation (dashed blue line in Figure 5 A), this is a highly challenging experiment. The DSC cell corresponds to a fixed bed reactor. In inert atmosphere, melting is observed at 409 °C (red curve in Figure 5 A). Under reaction conditions the evolved heat flow increases with temperature due to the exothermic propane oxidation (black and dashed blue lines in Figure 5 A). Above 400 °C, an endothermic signal starts due to the phase transition from solid to liquid with a clear peak at 409 °C. Simultaneously, the conversion of propane drops (Figure 5 B) and the selectivity to propylene increases (Figure 5 C). The catalytic profile recorded in the DSC cell perfectly resembles the one measured in a fixed-bed reactor (Figure S8 in the Supporting Information), although the measurement in the DSC cell was performed at lower contact time. Since the contact time in the fixed bed reactor was six times higher than in the operando DSC experiment, the conversion in the latter was much lower. The excellent agreement between the melting temperature and the change in performance shows that the effect in catalysis is clearly related to melting (Figure 5).

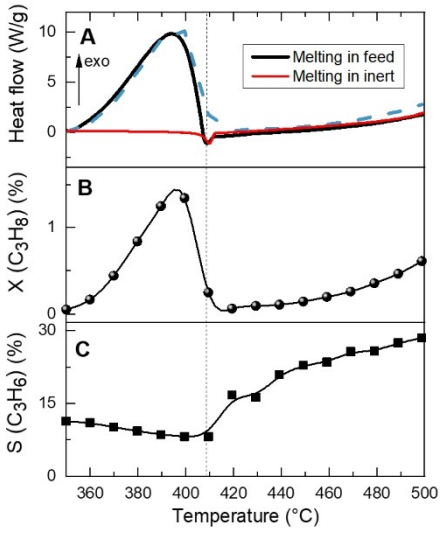

Figure 5. Operando- DSC profile of the catalyst K/V = 0.6 in propane oxidation; **(A)** Simultaneously measured heat flow with increasing temperature (dashed line: calculated heat flow based on on-line product analysis), **(B)** conversion of propane and **(C)** selectivity to propylene; Reaction conditions: total flow: 9 ml min^{-1}, feed: $C_3H_8/O_2/N_2$ = 7.5/7.5/85 vol%, GHSV = 4300 h^{-1}, β = 0.42 °C·min^{-1}, W/F = 0.34 g·s·ml^{-1}.

The drop in propane conversion could be caused by a drastic decrease in the specific surface area during melting, *e.g.*, by plugging pores or smoothing a rough surface. Therefore, a catalysis experiment was performed, stopped right after the drop and the catalyst was removed to analyze the surface area at this point (Figure S9 in the Supporting information). The observed decrease in specific surface area was only 20% (Table S2 in the Supporting Information), while the consumption rate of propane decreased from 8.1 µmol·g^{-1}·s^{-1} to 0.3 µmol·g^{-1}·s^{-1}, which corresponds to a reduction of 96% (Figure S9, Table S2). Thus, a reduction in the specific surface area of the catalyst during melting does not explain the observed decrease in activity.

The pure, unsupported potassium pentavanadate $K_3V_5O_{14}$ showed no activity in propane oxidation, neither in the solid nor in the molten state (Figure S10 in the Supporting Information). Consequently, melting of the inactive phase itself does not lead to any changes in performance.

Reference Experiments

As another explanation we can now assume that the only active species in the catalyst are dispersed vanadium oxide species detected by Raman spectroscopy (Figure S7 in the Supporting Information) and these species are then covered by the melt. To test this hypothesis, vanadium oxide supported on mesoporous silica SBA-15 (5.6 wt% V)[47–48] was placed beneath a layer of support-free $K_3V_5O_{14}$ in a fixed bed reactor (Figure S11 in the Supporting Information). The changes in activity and selectivity are consistent with the changes observed when measuring the K/V = 0.6 catalyst (compare Figure 5 with Figure S11 in the Supporting Information). Here it becomes evident from the reactor images in Figure S11 that the molten potassium vanadate phase covers the entire catalyst bed after heating above the melting point of $K_3V_5O_{14}$. We thus attribute the decrease in activity to the flooding of highly-active silica-supported V_xO_y centers, called in the following the "supported active species", with melt.

The simultaneous increase in selectivity is not solely due to the decrease of conversion. This is shown by an experiment (Figure S13 in the Supporting Information) in which the contact time was first varied on the solid catalyst and then on its liquefied state at the same temperature of 390 °C. When heated from room temperature to this low temperature, the surface

layer is still solid (see DSC results in Figure S12 in the Supporting Information) and at conversions between 0.5 and 3% the selectivity to propylene is 25% (Figure S13 in the Supporting Information). Then, the surface layer was completely liquefied by heating the catalyst to a reaction temperature of 500 °C. Subsequently, the catalyst bed was cooled down again to 390 °C. However, this did not result in solidification of the surface layer as a supercooled melt was formed (see the hysteresis in the heating and cooling cycles measured by DSC shown in Figure S12 in the Supporting Information), *i.e.*, the phase remains in a thermodynamically metastable liquid state. At this point, the contact time was varied again and slightly higher selectivity to propylene than over the solid catalyst can be detected over the supercooled melt at the same reaction temperature and conversion (Figure S13 in the Supporting Information).

Impact of Melting on Catalysis

In summary, adding alkali metal ions to silica-supported vanadium oxide allows the formation of alkali-vanadate phases that melt at the reaction temperatures of alkane oxidation. The melting then has an influence on the catalyst performance. The low activity of the melt (Figure 5B) could be attributed to the lack of strain in the V-O bonds in the species that are present at the liquid-gas interface.[3] To investigate this, a model catalyst containing supported $K_3V_5O_{14}$ as the only crystalline phase was prepared. However, besides $K_3V_5O_{14}$, additional highly dispersed vanadium oxide species V_xO_y of different nuclearity x bound to SiO_2 are present in K/V = 0.6 as well (Figure S7).[21] While the potassium vanadate phase seems to be completely inactive during propane oxidation in the solid and the liquefied states (Figure S10), the activity of K/V = 0.6 could only be due to the dispersed, SiO_2-bound vanadium oxide species, which corresponds to supported active species. This hypothesis is strengthened by the "flooding" experiment shown in Figure S11 and by the similar trend of the increase in propane conversion with increasing temperature and the comparable selectivity for V/SiO_2 and K/V = 0.6 in the solid state (Figure S14). After melting, the activity of the V_xO_y centers on the supported catalyst V/SiO_2 (in the "flooding" experiment, Figure S11) and K/V = 0.6 (Figures 5 and S14) is almost extinguished by covering the supported active species with molten alkali vanadate with the result that undesired subsequent reactions of propylene are prevented, and the selectivity remains high even with increasing conversion at higher temperatures (Figure S14).

Since K/SiO_2 has the highest activity among the two potassium-containing catalysts above the temperature of liquefaction of $K_3V_5O_{14}$ (Figure S14), the activity at higher temperatures seems to be controlled by potassium rather than vanadia, which further underlines the coverage of the supported active species (highly-active surface vanadium oxide species) by the melt.

At the high temperatures required for melting, it also can be assumed that homogeneous reactions in the gas phase provide an additional contribution to the activity. The molten layer itself may also play a role in releasing active radicals to initiate gas-phase hydrocarbon reactions.[49] If so, the catalyst generates alkyl fragments that further react to olefins in the gas-phase,[50–51] or OH radicals that contribute to selective dehydrogenation of propane to propylene.[52] In this study, a significant change in activation energies before and after melting suggests a difference in the reaction mechanism as one factor responsible for higher propylene selectivity in the liquified state (Arrhenius plots are presented in Figure S15, and apparent activation energies are listed in Table S3 in the Supporting Information). The apparent activation energy of 134 $kJ \cdot mol^{-1}$ calculated for both K/V = 0.6 in the liquid state and for SiO_2 in the same reaction temperature range further underlines the significant contribution of gas-phase reactions. On the other hand, since the same products were obtained before and after melting (Figure S16 in the Supporting Information), the change in the distribution of these products suggests that a significant difference in reaction rate constants must occur upon liquefaction, which could also be related to a change in the adsorption centers on the surface during melting. We can therefore not exclude that both factors, on the one hand the change of the surface centers, and on the other hand gas phase contributions, account for the change of reactivity.

The influence of alkali addition to supported vanadium oxide catalysts on the physicochemical and catalytic properties is complex and depends on the composition, the support, and the catalyst synthesis. In the oxidative dehydrogenation of propane to propylene, a decrease in activity and an increase in selectivity to propylene were most frequently observed in the literature.[9,30, 53] The effects were attributed to an influence of the alkali oxide on the reducibility,[21,54–55] and/or the acid-base properties.[54–55] Geometric and electronic effects[33] or an impact on the dispersion of the vanadium oxide species[31] were also discussed. The formation of alkali vanadates has been observed in related catalyst systems,[11,27, 56] and the melting was experimentally confirmed in catalysts studied for the oxidation of diesel soot.[56]

K-V compounds can also form locally in low concentrations, even if they are not detectable by XRD. However, although the melting temperatures of alkali vanadates are in the range of the reaction temperatures commonly used in oxidation reactions of hydrocarbons (400–550 °C), the effects of melting on catalytic properties have never been discussed in propane oxidation over alkali-doped vanadium oxide catalysts. In hotspots, which are to be expected due to the exothermicity of oxidation reactions, even higher temperatures can be reached. A strong indication of melting effects may be a progressive increase in selectivity to propylene with increasing propane conversion, as the present study also demonstrates (Figures 5 and S8 in the Supporting Information).

Conclusions

Liquefied surface layers can have highly interesting catalytic properties, especially for dehydrogenating alkanes to olefins.[57–58] This article aims to demonstrate, using a model

catalyst, the huge impact phase transformations can have on the performance and the reaction mechanism. Operando DSC and reference experiments clearly demonstrated that the non-oxidative melt of an alkali vanadate covers supported active species and extinguishes their activity. It becomes clear that the sudden change in catalyst performance upon melting is not directly associated with the transformation of the crystal structure of the predominating crystalline phase. Nor is it a chemical phenomenon, such as the degradation of strain through melting,[3] but a physical effect – the covering of the actual supported active species V_xO_y/SiO_2. Using the present example, our study highlights how to prove a supposed but misleading "obvious" structure-function relationship.

The results shed new light on the interpretation of doping effects of alkali elements in vanadium catalysts for selective oxidation and open further perspectives for improving selectivity in oxidation catalysis. The underlying catalyst dynamics are not always easy to capture analytically in real high-performance catalysts. Phase transformations at reaction temperatures must be considered when interpreting the effects of additives depending on the thermodynamic and solid-state kinetic properties of the active phase. We illustrate how a phase transition can lead to deactivation, with the positive side effect that the resulting melt covers highly-active centers for undesired consecutive reactions. These reactions are thus suppressed, even if higher conversions are reached at higher reaction temperatures. As a result, we generally postulate that high yields of the desired product could ultimately be achieved over liquified redox-inactive surface layers. Hence melting and targeted blocking of highly-active sites can also be considered as a design element for catalyst optimization.

Experimental

Chemicals

K_2CO_3 (>99%, Sigma Aldrich), V_2O_5 (>99%, BASF), and conventional amorphous silica (Aerosil 300, Degussa; 285 $m^2 g^{-1}$) were applied as starting materials. All chemicals were dried overnight at 80 °C before using. Millipore® water was used as solvent. Propane with a purity of 99.95% was purchased from Westfalen AG for the catalytic reaction. The purity of nitrogen, oxygen and argon was 99.999%.

Synthesis

The silica-supported K/V = 0.6 catalyst was prepared from a suspension of 0.3 g K_2CO_3, 0.7 g V_2O_5 and 9 g SiO_2 (Aerosil 300, ID S28958) in distilled water (350 ml). The suspension was stirred for 2 hours at room temperature and subsequently spray-dried applying the following parameters: T^{inlet} = 200 °C, T^{outlet} = 130 °C, aspirator = 100%, nozzle cleaner = 1, pump rate = 15%. The obtained fine powder (ID S28600) was transferred to a rotating quartz tube and calcined in synthetic air (21 vol% O_2 in N_2) using a flow rate of 10 ml·min^{-1} at 620 °C (heating rate 2 °C·min^{-1}) for 16 hours. After cooling down to room temperature, ~6 g of catalyst were obtained (internal ID is S28654). A total metal oxide content of 10 wt% was targeted. Silica-supported potassium (ID S28690) and vanadium (ID S28683) oxides were synthesized as reference catalysts according to the same procedure.

For reference, the support-free $K_3V_5O_{14}$ was prepared using a conventional solid-state method described elsewhere.[59] For this, 3 g K_2CO_3 and 6 g V_2O_5 were mixed and ground in a mortar. The solid mixture was pressed into pellets (3 cm diameter) with 2 tons for 1 min. Prepared pellets were transferred into a tube furnace (Carbolite) and heated to 380 °C (heating rate 10 °C·min^{-1}) in flowing 21 vol% O_2 in Ar. After the temperature was reached, the pellets were kept at this temperature for 4 days and then cooled down to room temperature at the natural rate of cooling in the tube furnace. The procedure was repeated several times until the target phase was reached (internal ID is S31564).

Characterization

The phase composition of catalysts was identified by X-ray diffraction (XRD) using a Bruker D8 ADVANCE II theta/theta diffractometer. Ni-filtered Cu Kα radiation and a position-sensitive LynxEye silicon strip Detector were applied. The XRD data were analyzed by full pattern Rietveld fitting using the TOPAS software (TOPAS, Version 6, Bruker AXS).

The potassium and vanadium contents of the materials were determined by X-ray Fluorescence (XRF) using the Pioneer S4 (Bruker AXS GmbH) spectrometer. For sample preparation, a mixture of 0.05 g catalyst and 8.9 g lithium tetraborate (>99.995%, Aldrich) was fused into a disk using an automated fusion machine (Vulcan 2 MA, Fluxana). Calibration was performed using the physical mixtures of K_2O and SiO_2 in various ratios.

Ambient pressure X-ray photoelectron spectroscopy (AP-XPS) was carried out at the BElChem (Berlin joint lab for electrochemical interfaces) beamline at the synchrotron radiation source BESSY II in Berlin, Germany. A pressed powder pellet (1 ton, 8 mm diameter) of about 15 mg supported catalyst on a SiC plate and a sapphire sample holder was activated, *i.e.*, heated under dynamic flow (21 vol% O_2 in N_2) at 10 °C·min^{-1} to 520 °C and held there for 2 hours. Si 2p, O 1s, and V 2p XPS core level spectra were collected by setting the pass energy of the spectrometer to 20 eV. The excitation energy was 680 eV for O 1s and for V 2p, and 260 eV for Si 2p spectra. XPS core level spectra of K 2p were collected with a photon energy of 440 eV. Quantitative elemental abundance of O 1s and the V $2p_{1/2}$ and V $2p_{3/2}$ core levels were determined using tabulated atomic subshell photo-ionization cross sections.[60] The peaks were fitted with Gaussian-Lorentzian functions after a Shirley background correction within the CASA data analysis software. The total peak areas of the respective core levels after a Shirley background correction were taken for calculation of the average oxidation state. For vanadium, the sum of V $2p_{1/2}$ and V $2p_{3/2}$ areas was used. To minimize differential charging, the spectra were collected 520 °C.

The specific surface area was determined applying the multipoint Brunauer – Emmett – Teller (BET) method based on N_2 adsorption-desorption isotherms recorded at −196 °C using an Autosorb AS-6B (Quantachrome) analyzer. The sample was degassed in dynamic vacuum at a temperature of 150 °C for 2 h prior to adsorption. Adsorption isotherms with 11 data points were recorded and the linear range of the adsorption isotherm ($0.05 < p/p_0 < 0.15$) was considered for data analysis assuming a N_2 cross-sectional area of 16.2 Å^2.

The thermal behavior of catalysts regarding phase transitions was studied in a heat flux differential scanning calorimeter (DSC) (Mettler-Toledo HP DSC 827) with a star-shaped, layered Au–Au-Pd sensor (one layer 56 thermocouples). The measurements were

carried out under a dynamic atmosphere 21 vol% O_2/79 vol% Ar (70 ml·min^{-1}) with a heating rate of 10 °C·min^{-1} and a cooling rate of 5 °C·min^{-1}. To test for reversibility of the endothermic processes, three heating and cooling cycles were applied. The temperatures and heat flows were calibrated by measuring the melting points of certified indium and zinc specimens.

The content of potassium vanadate in supported K/V = 0.6 (internal ID S28654) was determined using the melting enthalpy of support-free $K_3V_5O_{14}$ (internal ID 31564) as reference. The content of pentavanadate $K_3V_5O_{14}$ in the SiO_2-supported catalyst determined in this way is 5.2 wt%. The deviation from the value of 8.2 wt% determined by XRF analysis is due to the reaction of K with silica and the formation of amorphous vanadium oxide species.

Raman measurements were conducted using a TriVista Raman Microscope System (TriVista TR 557, S&I, GmbH) equipped with a liquid N_2-cooled CCD camera (Spec10: 100BR, Princeton Instruments) applying two different laser wavelengths, namely, 266 nm and 532 nm. The 266 nm laser used was from CryLas (266 nm, FQCW 266) and the beam was focused with a 15x objective, applying a laser power of 0.41 mW. For the 532 nm laser (DPSS Lasers (Cobolt 05–01 series)), the beam was focused with a 10x objective (Olympus), applying a laser power of 2 mW at the sample position. No beam damage was observed under these conditions. The measurements were performed after pre-treatment of the samples in a Linkam CCR1000 (Linkam Scientific, Tadworth, UK) cell using a flow of 1 ml·min^{-1} of 21 vol% O_2 diluted in nitrogen in the temperature range from 50 °C to 520 °C. Spectra acquisition was performed in 10 accumulations of 60 seconds each (t = 10 min) for the 532 nm laser, whereas 30 accumulations of 60 seconds each (t = 30 min) were necessary by measuring with the 266 nm laser. The temperature was accurately controlled by the Linkam T96.S controller (via a S-type platinum/rhodium thermocouple). Temperature calibration in the cell was done by measuring the melting point of potassium pentavanadate crystals ($K_3V_5O_{14}$) under 10 ml·min^{-1} flow of synthetic air (21 vol% O_2 balanced by N_2).

Oxidative Dehydrogenation of Propane

Propane oxidation was measured in a commercial parallel reactor setup (Premex Reactor GmbH) composed of two reactor blocks with 8 fixed-bed reactors at atmospheric pressure. The catalysts were pressed under 0.0196 MPa and sieved into a particle size of 250–355 μm. Quartz wool was placed at the tapering point of the empty reactor in order to hold the catalyst bed in the isothermal zone of the reactor. 350 mg of catalyst was loaded without dilution. The thermocouple for temperature measurements was placed coaxially in the catalyst bed. The temperature was varied between 350 °C and 520 °C. An empty reactor with SiO_2 (Aerosil 300, particle size: 250–355 m was used to check the inertness of the support. All catalysts were activated in an oxidative atmosphere (21 vol% O_2 balanced by N_2) at 520 °C (heating rate 2 °C·min^{-1}) for 2 h, followed by cooling to 50 °C. Then, the catalysts were exposed to the reaction mixture containing C_3H_8, O_2 and N_2 in a ratio of 7.5:7.5:85 vol% using mass flow controllers (Bronkhorst USA, Inc.). A precise total gas flow of 10 mL·min^{-1} was fed to start the reaction. Product analysis was performed using an Agilent 7890 A GC system equipped with thermal conductivity (TCD) and flame ionization detectors (FID). A combination of Plot-Q (length 30 m, 0.53 mm internal diameter, 40 μm film thickness) and Plot-MoleSieve 5 A (30 m length, 0.53 mm internal diameter, 50 μm film thickness) columns, connected to the thermal conductivity detector (TCD), was used to analyze the permanent gases CO, CO_2, N_2, O_2, and CH_4. A system of a FFAP (length 30 m, 0.53 mm internal diameter, 1 μm film thickness) and a Plot-Q column (length 30 m, 0.53 mm internal diameter, 40 μm film thickness), connected to a flame ionization detector (FID), was used to analyze C_2-C_3 hydrocarbons and oxygenates. The catalyst was kept at each reaction temperature for 24 h until steady state was achieved. Propylene and carbon oxides (CO and CO_2) were found as main reaction products. The amounts of C_2 products and oxygenates (acrolein, acrylic acid and propionaldehyde) were below 2% of the total amount of products. The SiO_2 support can be regarded as inactive under the applied reaction conditions since the conversion of propane at the highest temperature (*i.e.*, 520 °C) was found to be 1.7%. The conversion of propane X and the selectivity to product j S_j were calculated based on the sum of products according to Eq. (1) and (2), respectively:

$$X = \frac{\sum_{j=1}^{n} N_j c_j}{N_{alkane} c_{alkane,0}} \times 100 \quad (1)$$

$$S_j = \frac{\frac{N_j}{N_{alkane}} c_j}{\sum_{j=1}^{n} \frac{N_j}{N_{alkane}} c_j} \times 100 \quad (2)$$

where N_j is the number of carbon atoms in the product j, c_j is the concentration of product j in the gas at the reactor exit, N_{alkane} is the number of carbon atoms in the alkane, $c_{alkane,0}$ is the concentration of the alkane in the reactant feed.

Reaction rates for propane consumption and propylene formation were determined by using the following Eq. (3):

$$\frac{d(n_i)}{d\left(W/F\right)}) = \vartheta_i r_i \quad (3)$$

where n_i is the number of alkane at the reactor exit, W is the mass of the catalyst in g, F is the total flow rate of the inlet gas stream, and ϑ_i is the stoichiometric coefficient of alkane. The rates are normalized to the vanadium content in g and provided in the unit $mol\ g^{-1}{}_V s^{-1}$. For the calibration procedure, please see the operando DSC section below.

Operando Differential Scanning Calorimetry (DSC)

Operando thermal analysis was studied using a Calvet type[61] *in situ* calorimeter with plug-flow geometry Sensys Evo (Setaram) coupled with a gas chromatograph Agilent 7890B and custom-designed mass-spectrometer (Pfeiffer Vacuum). The (PtRh-Pt) Calvet type sensor was calibrated on the production site with contact-free Ohm resistance and verified against melting enthalpy of a certified indium standard. A volume of approximately 125 μl sample was pressed under 0.0196 MPa and sieved (sieve fraction 100-250 μm).

Approximately 50 mg of sample was loaded into a 150 mm long quartz tube with an inner diameter of 4 mm and placed on a sintered glass substrate covered with a thin layer of quartz wool (10 mm batch length, 125 μl batch volume) in the center of the measurement zone of the calorimeter. An identical reactor was used in the reference position of the calorimeter. The reference reactor was filled with quartz wool and kept under continues N_2 flow equal to the total flow on the sample side. The gas chromatograph was coupled with the calorimeter downstream of the reactor. Injected through the preheated inlet the solute was split and introduced into two channels: a thermal conductivity detector (TCD) for the analysis of CO, CO_2, Ar, O_2 via HP Plot Q (30 m, 0.53 mm I.D., 40 m and HP Molsieve 5 A (30 m, 0.53 mm I.D., 50 m capillary columns, and a flame ionization detector (FID) for detecting C_3H_8 and C_3H_6 via HP Plot Q and HP FFAP (30 m x

0.53 mm x 1.0 m columns. The complete separation run lasted 22 min. Thus, to acquire the product concentration at every 10 °C the heating rate of 0.42 °C·min^{-1} was adjusted for the DSC experiment. All connection lines were permanently held at 120 °C to avoid condensation. Quantitative calibration was performed for CO_2 with multiple concentrations (0.25–20 %). Each calibration test had five repetitions, which were then averaged. Excellent linearity in the analyzed concentration range was achieved with 5 points. For calibration of C_3H_6, C_3H_8, CO, O_2 certified calibration mixtures with the following content: 2 % C_3H_6, 5 % C_3H_8, 1 % CO, and 1 % O_2 were used. The controlled gas flow was maintained with mass flow controllers EL-Flow by Bronkhorst, additionally calibrated with a flowmeter Definer 220.

Owing to the heat capacity *(C_p)* of the sample, there would be a temperature difference of the heat transferred to the sample and the reference reactor. The difference is measured by the thermocouples and represented as *dQ/dt*. The change in number of molecules of the outlet stream is recorded by GC and represented as *dN/dt*. The general equation for the calculation of the heat flow for a sample is as follows:

$$q = \left(\frac{dQ}{dt}\right) / \left(\frac{dN}{dt}\right) \quad (4)$$

where *dQ/dt* is the total heat flow and *dN/dt* is the change in the number of molecules at the reactor exit.

Catalysts were first activated in an oxidative environment with 9 mLmin^{-1} total flow (21 vol % O_2 in N_2) at 620 °C (heating rate = 10 °C·min^{-1}) for 2 h then completely cooled down with 10 °C·min^{-1} in the same gas feed. For the reaction, the total flow of 9 mL·min^{-1}, $C_3H_8/O_2/N_2$-7.5/7.5/85 (M_{cat}/F_{total} = 0.34 g·s·ml^{-1}, GHSV ≈4300 h^{-1}) was adjusted and a temperature ramp (β = 0.42 °C·min^{-1}) applied. In contrast to the experiment in a fixed bed reactor, we deliberately lowered the contact time to reduce the propane conversion and thus the exothermic effect of the reaction.

Calculation of the heat flow generated by the reaction was calculated based on the rates of C_3H_6 and CO_x formation and standard reaction enthalpies calculated for stoichiometric reactions per mol of propane. The calculated heat flow (HF) in J·min^{-1}·g^{-1} is defined as follows:

$$-HF = r_{C_3H_6} \times \Delta H^0_{r(C_3H_6)} + r_{CO_2} \times \Delta H^0_{r(CO_2)} + r_{CO} \times \Delta H^0_{r(CO)} \quad (5)$$

where r_i are formation rates in mol·min^{-1}g^{-1} and $\Delta H^0_{r(i)}$ is a reaction enthalpy form tabulated enthalpies of formation in Jmol^{-1} (C_3H_8). The temperature effect on enthalpies were neglected.

$$C_3H_8 + 0.5O_2 \rightarrow C_3H_6 + H_2O \quad \Delta H^0_{r(C_3H_6)} = -116.7 kJ/mol(C_3H_8) \quad (6)$$

$$C_3H_8 + 5O_2 \rightarrow 3CO_2 + 4H_2O \; \Delta H^0_{r(CO_2)} = -2043 \; kJ/mol(C_3H_8) \quad (7)$$

$$C_3H_8 + 3.5O_2 \rightarrow 3CO + 4H_2O \quad \Delta H^0_{r(CO)} = -1194 \; kJ/mol(C_3H_8) \quad (8)$$

In situ X-Ray Diffraction

XRD scans were conducted using a Theta/theta X-ray diffractometer with Bragg-Brentano geometry (STOE). Cu $K_{\alpha 1+2}$ irradiation was used; a secondary graphite monochromator (graphite) was installed, and a scintillation counter measured the diffracted beam. The sample was placed as a pellet on the top of an Al foil in the sample holder of an Anton Paar XRK 900 heating chamber. Close to the sample, a thermocouple measured the set temperature. The Al foil ensured correct height of the sample with respect to the beam position. The XRK 900 in situ chamber was open and thus flooded with air. The sample was heated at 10 °C·min^{-1} to the desired temperature. At each temperature an XRD pattern was measured for approximately 11 h per scan. Cooling was performed at 5 °C·min^{-1}. Heating and cooling cycles were performed 3 times in a row. During the 2nd and 3rd heating cycle the scan range was increased to observe more reflexes yielding in a scan time of about 17 h. Due to melting and recrystallization, some sample moved out of the beam position causing a drop in the intensity in the 2nd and further in the 3rd heating cycle

Acknowledgements

This study has been conducted in collaboration between the Fritz-Haber-Institut der Max-Planck-Gesellschaft (https://www.fhi.mpg.de), the BasCat- UniSysCat BASF Joint Lab (https://www.bascat.tu-berlin.de/bascat/menue/bascat) and the Technical University Berlin (https://www.tu.berlin/en/). We thank Dr. Frank Girgsdies for XRD, Maike Hashagen for nitrogen adsorption, Dr. Olaf Timpe for XRF measurements, and Danail Ivanov and Wiebke Frandsen for SEM investigations. We also thank Jasmin Allan and Sven Richter for their technical assistance. Open Access funding enabled and organized by Projekt DEAL.

Conflict of Interests

The authors declare no conflict of interest.

Data Availability Statement

The data that support the findings of this study are available in the supplementary material of this article.

Keywords: alkali · melting · vanadium · oxidation · propane

[1] A. Khorshidi, J. Violet, J. Hashemi, A. A. Peterson, *Nature Catalysis* **2018**, *1*, 263.
[2] S. A. Akhade, J. R. Kitchin, *J. Chem. Phys.* **2012**, *137*, 084703.
[3] K. Amakawa, L. Sun, C. Guo, M. Hävecker, P. Kube, I. E. Wachs, S. Lwin, A. I. Frenkel, A. Patlolla, K. Hermann, R. Schlögl, A. Trunschke, *Angew. Chem. Int. Ed.* **2013**, *52*, 13553.
[4] G. A. Somorjai, *Catal. Lett.* **1992**, *12*, 17.
[5] B. Zugic, L. Wang, C. Heine, D. N. Zakharov, B. A. J. Lechner, E. A. Stach, J. Biener, M. Salmeron, R. J. Madix, C. M. Friend, *Nat. Mater.* **2017**, *16*, 558.
[6] M. J. Werny, Y. Wang, F. Girgsdies, R. Schlögl, A. Trunschke, *Angew. Chem. Int. Ed.* **2020**, *59*, 14921.
[7] V. Muravev, J. F. M. Simons, A. Parastaev, M. A. Verheijen, J. J. C. Struijs, N. Kosinov, E. J. M. Hensen, *Angew. Chem. Int. Ed.* **2022**, *61*, e202200434.
[8] G. Ertl, *Angew. Chem. Int. Ed.* **2008**, *47*, 3524.
[9] A. A. Lemonidou, L. Nalbandian, I. A. Vasalos, *Catal. Today* **2000**, *61*, 333.
[10] A. Klisińska-Kopacz, I. Gressel, B. Grzybowska, M. Mikołajczyk, J. Stoch, *Pol. J. Chem.* **2006**, *80*, 825.
[11] M. Nadjafi, P. M. Abdala, R. Verel, D. Hosseini, O. V. Safonova, A. Fedorov, C. R. Müller, *ACS Catal.* **2020**, *10*, 2314.

[12] R. Grabowski, B. Grzybowska, K. Samson, J. Słoczyński, J. Stoch, K. Wcisło, *Appl. Catal. A* **1995**, *125*, 129.
[13] C. Resini, M. Panizza, L. Arrighi, S. Sechi, G. Busca, R. Miglio, S. Rossini, *Chem. Eng. J.* **2002**, *89*, 75.
[14] T. Blasco, J. M. Lopez Nieto, *Appl. Catal. A* **1997**, *157*, 117.
[15] F. Cavani, N. Ballarini, A. Cericola, *Catal. Today* **2007**, *127*, 113.
[16] Y. Gambo, S. Adamu, A. A. Abdulrasheed, R. A. Lucky, M. S. Ba-Shammakh, M. M. Hossain, *Appl. Catal. A* **2021**, *609*, 117914.
[17] C. A. Gärtner, A. C. van Veen, J. A. Lercher, *ChemCatChem* **2013**, *5*, 3196.
[18] R. Grabowski, *Catalysis Reviews: Science and Engineering* **2006**, *48*, 199.
[19] J. T. Grant, J. M. Venegas, W. P. McDermott, I. Hermans, *Chem. Rev.* **2018**, *118*, 2769.
[20] C. Hess, *ChemPhysChem* **2009**, *10*, 319.
[21] C. A. Carrero, R. Schlögl, I. E. Wachs, R. Schomäcker, *ACS Catal.* **2014**, *4*, 3357.
[22] G. G. Cortez, J. L. G. Fierro, M. A. Banares, *Catal. Today* **2003**, *78*, 219.
[23] A. Klisińska, A. Haras, K. Samson, M. Witko, B. Grzybowska, *J. Mol. Catal. A* **2004**, *210*, 87.
[24] A. Klisińska, S. Loridant, B. Grzybowska, J. Stoch, I. Gressel, *Appl. Catal. A* **2006**, *309*, 17.
[25] A. Klisińska-Kopacz, I. Gressel, B. Grzybowska, M. Mikołajczyk, J. Stoch, *Pol. J. Chem.* **2006**, *80*, 825–833.
[26] D. Courcot, B. Grzybowska, Y. Barbaux, M. Rigole, A. Ponchel, M. Guelton, *J. Chem. Soc. Faraday Trans.* **1996**, *92*, 1609.
[27] D. Courcot, A. Ponchel, B. Grzybowska, Y. Barbaux, M. Rigole, M. Guelton, J. P. Bonnelle, *Catal. Today* **1997**, *33*, 109.
[28] A. Galli, J. M. López Nieto, A. Dejoz, M. I. Vazquez, *Catal. Lett.* **1995**, *34*, 51.
[29] G. Garcia Cortez, J. L. G. Fierro, M. A. Bañares, *Catal. Today* **2003**, *78*, 219.
[30] R. Grabowski, B. Grzybowska, A. Kozłowska, J. Słoczyński, K. Wcisło, Y. Barbaux, *Top. Catal.* **1996**, *3*, 277.
[31] J. T. Grant, C. A. Carrero, A. M. Love, R. Verel, I. Hermans, *ACS Catal.* **2015**, *5*, 5787.
[32] Q. Liu, M. Luo, Z. Zhao, L. Guo, *Catal. Lett.* **2019**, *149*, 1345.
[33] M. Calatayud, C. Minot, *J. Phys. Chem. C* **2007**, *111*, 6411.
[34] L. Y. Margolis, A. A. Firsova, *Int. Rev. Phys. Chem.* **1989**, *8*, 1.
[35] R. Grabowski, *Appl. Catal. A* **2004**, *270*, 37.
[36] R. Grabowski, J. Słoczyński, *Chem. Eng. Process.* **2005**, *44*, 1082.
[37] B. Grzybowska-Świerkosz, *Top. Catal.* **2002**, *21*, 35.
[38] A. P. S. Dias, L. D. Dimitrov, M. C.-R. Oliveira, R. Za˘voianu, A. Fernandes, M. F. Portela, *J. Non-Cryst. Solids* **2010**, *356*, 1488.
[39] Z. Zhao, L. Jian, A. Duan, X. Chunming, T. Kobayashi, I. Wachs, *Top. Catal.* **2006**, *38*, 309.
[40] Z. Zhao, J. Liu, A. J. Duan, C. M. Xu, T. Kobayashi, I. E. Wachs, *Top. Catal.* **2006**, *38*, 309.
[41] F. Holtzberg, A. Reisman, M. Berry, M. Berkenblit, *J. Am. Chem. Soc.* **1956**, *78*, 1536.
[42] Y.-Q. Chen, L. Li, Q. Ren, H.-T. Zhu, J.-K. Liang, J. Luo, J.-B. Li, G.-H. Rao, *Chinese Physics B* **2011**, *20*, 076402.
[43] G. Mestl, T. Ilkenhans, D. Spielbauer, M. Dieterle, O. Timpe, J. Kröhnert, F. Jentoft, H. Knözinger, R. Schlögl, *Appl. Catal. A* **2001**, *210*, 13.
[44] J. Zemek, P. Jiricek, O. Gedeon, B. Lesiak, A. Jozwik, *J. Non-Cryst. Solids* **2005**, *351*, 1665.
[45] R. Sawyer, H. W. Nesbitt, R. A. Secco, *J. Non-Cryst. Solids* **2012**, *358*, 290.
[46] D. Maganas, A. Trunschke, R. Schlögl, F. Neese, *Faraday Discuss.* **2016**, *188*, 181.
[47] P. Gruene, T. Wolfram, K. Pelzer, R. Schlögl, A. Trunschke, *Catal. Today* **2010**, *157*, 137.
[48] P. Kube, B. Frank, S. Wrabetz, J. Kröhnert, M. Hävecker, J. Velasco-Vélez, J. Noack, R. Schlögl, A. Trunschke, *ChemCatChem* **2017**, *9*, 573.
[49] K. Takanabe, A. M. Khan, Y. Tang, L. Nguyen, A. Ziani, B. W. Jacobs, A. M. Elbaz, S. M. Sarathy, F. Tao, *Angew. Chem. Int. Ed.* **2017**, *56*, 10403.
[50] L. Leveles, K. Seshan, J. A. Lercher, L. Lefferts, *J. Catal.* **2003**, *218*, 296.
[51] L. Leveles, K. Seshan, J. A. Lercher, L. Lefferts, *J. Catal.* **2003**, *218*, 307.
[52] P. Kube, J. Dong, N. S. Bastardo, H. Ruland, R. Schlögl, J. T. Margraf, K. Reuter, A. Trunschke, *Nat. Commun.* **2022**, *13*, 7504.
[53] J. T. Grant, A. M. Love, C. A. Carrero, F. Huang, J. Panger, R. Verel, I. Hermans, *Top. Catal.* **2016**, *59*, 1545.
[54] Z. Zhao, Y. Yamada, A. Ueda, H. Sakurai, T. Kobayashi, *Catal. Today* **2004**, *93–95*, 163.
[55] Y. Li, Z. Wei, J. Sun, F. Gao, C. H. F. Peden, Y. Wang, *J. Phys. Chem. C* **2013**, *117*, 5722.
[56] Z. Zhao, J. Liu, A. Duan, C. Xu, T. Kobayashi, I. E. Wachs, *Top. Catal.* **2006**, *38*, 309.
[57] T. Bauer, S. Maisel, D. Blaumeiser, J. Vecchietti, N. Taccardi, P. Wasserscheid, A. Bonivardi, A. Görling, J. Libuda, *ACS Catal.* **2019**, *9*, 2842.
[58] N. Taccardi, M. Grabau, J. Debuschewitz, M. Distaso, M. Brandl, R. Hock, F. Maier, C. Papp, J. Erhard, C. Neiss, W. Peukert, A. Görling, H. P. Steinrück, P. Wasserscheid, *Nat. Chem.* **2017**, *9*, 862.
[59] J. Yeon, S.-H. Kim, P. S. Halasyamani, *Inorg. Chem.* **2010**, *49*, 6986.
[60] J. J. Yeh, I. Lindau, *Atomic Data and Nuclear Data* **1985**, *32*, 1.
[61] E. J. P. Calvet, in *United States* (Ed.: U. States), US305947A, **1962**.

Manuscript received: October 20, 2023
Revised manuscript received: December 1, 2023
Accepted manuscript online: December 8, 2023
Version of record online: January 16, 2024